SCIENTIFIC REPORTS

OPEN

SUBJECT AREAS:
POROUS MATERIALS
DNA AND RNA
GELS AND HYDROGELS
BIOINSPIRED MATERIALS

Received
4 October 2012

Accepted
25 January 2013

Published
15 February 2013

Correspondence and requests for materials should be addressed to N.P. (n2010.park@samsung.com)

DNA hydrogel-based supercapacitors operating in physiological fluids

Jaehyun Hur[1], Kyuhyun Im[1], Sekyu Hwang[2], ByoungLyong Choi[1], Sungjee Kim[2], Sungwoo Hwang[1], Nokyoung Park[1] & Kinam Kim[3]

[1]Frontier Research Laboratory, Samsung Advanced Institute of Technology, Samsung Electronics, Yongin, Kyunggi-do 446-712, South Korea, [2]Department of Chemistry, Pohang University of Science & Technology, Pohang, 790-784, South Korea, [3]Samsung Advanced Institute of Technology, Samsung Electronics, Yongin, Kyunggi-do 446-712, South Korea.

DNA nanostructures have been attractive due to their structural properties resulting in many important breakthroughs especially in controlled assemblies and many biological applications. Here, we report a unique energy storage device which is a supercapacitor that uses nanostructured DNA hydrogel (Dgel) as a template and layer-by-layer (LBL)-deposited polyelectrolyte multilayers (PEMs) as conductors. Our device, named as PEM-Dgel supercapacitor, showed excellent performance in direct contact with physiological fluids such as artificial urine and phosphate buffered saline without any need of additional electrolytes, and exhibited almost no cytotoxicity during cycling tests in cell culture medium. Moreover, we demonstrated that the PEM-Dgel supercapacitor has greater charge-discharge cycling stability in physiological fluids than highly concentrated acid electrolyte solution which is normally used for supercapacitor operation. These conceptually new supercapacitors have the potential to be a platform technology for the creation of implantable energy storage devices for packageless applications directly utilizing biofluids.

DNAs have been utilized as building blocks for controlled assemblies of complicated molecular nanostructures[1–8]. DNA hydrogel (Dgel) is a recently developed biomaterial which has thinly layered porous structures made by enzymatic crosslinking of branched DNA monomers[9]. Owing to the dual nature of Dgel as DNA and hydrogel, it has synergistically combined physical and mechanical properties. In other words, because branched DNA is used as a building block, the nanostructure of Dgel can be precisely tunable by engineering the monomer units[9]. Simultaneously, because of its crosslinked hydrophilic three-dimensional network structure as a hydrogel, the surface-to-volume ratio is remarkably high[10–14]. Up until now, although several different researches using Dgel have mainly focused on biological applications including cell-free protein production, drug delivery, and live cell encapsulation, none of these have reported the utilization of Dgel as a component of electrochemical energy storage devices which is expected to have biocompatible properties[9,15,16]. At present, most of bio-related devices utilize external power sources or packaged conventional energy storage[17–21]. However, there have been no serious efforts to develop energy storage devices that satisfy the non-cytotoxicity and long-term functionality during the charging/discharging process[22].

Electrochemical capacitors (or supercapacitors) are the best candidates for energy storage devices that can be operated in bio-environments because it is easier to find biocompatible components and to exclude the electrochemical reactions for supercapacitors than for batteries or fuel cells[23–30]. Furthermore, because supercapacitors can directly utilize physiological fluid as a source of electrolyte, these devices can be potentially implanted inside fluid rich organs such as blood vessel, eyeball or bladder without cumbersome packages[31]. However supercapacitor which is even close to this aim has yet to be presented. We present herein Dgel based supercapacitors which can be operative on tissue and in physiological fluids (Fig. 1a). Our Dgel supercapacitor (PEM-Dgel) structure has been realized by adopting electrostatic interaction driven layer by layer (LBL) deposition. The functionalities of PEM-Dgel supercapacitors in biofluids such as phosphate-buffered saline (PBS) and artificial urine were assessed. More importantly, the cytotoxicity of our supercapacitor was evaluated using multiple charge-discharge experiments in cell culture medium.

Results

Construction of PEM-Dgel supercapacitor. Dgel is composed of layered porous network structure fabricated by enzymatic crossliking of X-shaped DNAs[9,15,16]. Specifically, X-shaped DNAs with 6 nm of each branch length were designed as monomer units and the resulting Dgel matrix has hierarchical pore structure with macropores

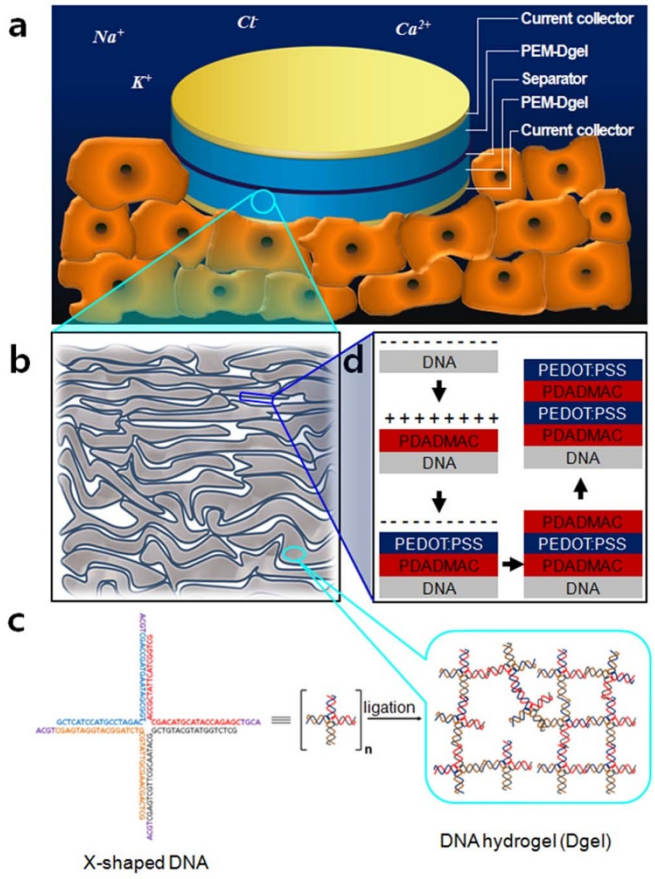

Figure 1 | PEM-Dgel supercapacitors. Schematic representation of, (a), PEM-Dgel supercapacitor operation in physiological environment (stacked features underneath the device display the cells). (b), Enlarged detailed structure of PEM-Dgel where porous layered Dgel (grey) is covered by conductive PEM (indigo), (c), Magnified view of Dgel where X-shaped double stranded DNAs are crosslinked by enzymatic reaction, (d), Construction of PEM-Dgel electrodes by coating the Dgel with the polyelectrolyte pair (PDADMAC/PEDOT:PSS) using LBL deposition.

(>1 um between each layered structure, Fig. 1b) and mesopores (~10 nm on layered area, Fig. 1c)[9]. In addition, the negative charges on Dgels provide an ideal substrate for the creation of functional materials when oppositely charged species are subsequently assembled onto these gels[32,33]. To build up energy storage layers in the Dgel, multiple layers of a pair of polyelectrolytes, poly (3,4-ethylenedioxythiophene):poly(styrenesulfonate) (PEDOT:PSS) and polydiallydimethyl-ammonium chloride (PDADMAC), were deposited using LBL process (Fig. 1d). The as-prepared dried Dgel consisted of a number of extremely thin, sheet-like domains that were assembled on one another (SEM images in Fig. 2a). At the periphery of the sheet-like structure, relatively thick wrinkle-like areas were also visible and appeared brighter than the other regions. The thickness of the sheet-like structure ranged from a few nanometers to tens of nanometers, whereas the wrinkle-like area measured tens to hundreds of nanometers thick. On the negatively charged wet Dgel surface, a single pair of PDADMAC/PEDOT:PSS was deposited via LBL deposition using electrostatic interactions, resulting in a conducting layer with almost the same morphology as the native Dgel (Fig. 2b). The effectiveness of the electrostatic LBL deposition in creating the polyelectrolyte double-layer coating was confirmed by the control experiments in which neutral agarose gel showed a non-uniform coating of PEDOT:PSS (Fig. S1). Special care was also required during the washing step between the polyelectrolyte depositions because Dgel is mechanically vulnerable due to its three dimensional, porous, and layered structure. The PEM-Dgel structure was well preserved even after the LBL deposition process was repeated five times on the same gel (Fig. S2).

Optical and electrical characterization of PEM-Dgel. The electrical and optical properties were measured to confirm the formation of the PEMs on the Dgel. The sheet resistance of the PEM-Dgel was inversely proportional to the number of PEMs, which indicates that all of the PEMs on the Dgel surface participate in conduction (Fig. 2c). When five PEM bilayers were built up, the sheet resistance decreased to as low as 66 ± 6 ohm/sq. This low sheet resistance was also due to the unique thin and porous structure of the Dgel. The Raman spectrum of the PEM-Dgel is presented in Fig. 2d. No Raman peaks corresponding to Dgel and PDADMAC were observed, but peaks were present at 1266, 1368, and 1440 cm^{-1}; these are the signature peaks of PEDOT:PSS[34]. These PEDOT:PSS peaks did not exhibit any shift, which suggests that no chemical changes occurred during the deposition process. The uniform distribution of PEDOT:PSS on the Dgel was revealed by EDS mapping of sulfur (Fig. 2e). These results confirm that the conductive component was successfully intercalated into the layered Dgel structure.

Electrochemical performance of PEM-Dgel supercapacitor in physiological fluids. The electrochemical properties of PEM-Dgel in biocompatible fluids were evaluated using both cyclic voltammetry and galvanostatic technique. PBS and artificial urine were selected as biocompatible fluids to evaluate the device's performance under physiological conditions. The cyclic voltammograms measured at different voltage scan rates are shown for PBS (Fig. 3a) and artificial urine (Fig. 3b) as electrolytes. In both fluids, symmetric CV curves were maintained for all scan rates applied (25 mV/s ~ 2000 mV/s). At 25 mV/s, the specific capacitances of PEM-Dgel were measured to be 13.4 ± 1.2 and 31.9 ± 2.4 F/g for PBS and artificial urine, respectively. The higher capacitance in artificial urine than in PBS is thought to result from the greater number of ionic species and their higher concentrations in the artificial urine. The dependence of specific capacitance (C_{sp}) on the voltage scan rate was almost identical for both fluids. For all scan rates applied, the relative capacitance values ($C_{sp,\ PBS}/C_{sp,\ artificial\ urine}$) were consistently ~0.4 (Fig. 3c). A commonly observed trend was that the specific capacitance radically decreased as the voltage scan rate increased (Fig. 3c). This trend is due to the ineffective ion accumulation on porous PEM-Dgel electrodes at high scan rates. Very similar behavior was observed for the galvanostatic measurements, for which the highest C_{sp} of 28.5 ± 2.2 F/g at 1 A/g in artificial urine was ~2.5 times greater than that of 11.5 ± 1.1 F/g in PBS at the same current density (Figs. 3d and 3e). The dramatic decrease in the specific capacitance as a function of the current density increase can also be explained by the inefficiency of ion accumulation.

Cytotoxicity test of PEM-Dgel supercapacitor. The cytotoxicity test of our supercapacitor (Au/PEM-Dgel/separator/PEM-Dgel/Au, Fig. 1a) was performed by electrochemical charge-discharge cycling on mouse embryonic fibroblast cells (NIH3T3 cells) immersed in cell culture medium (Minimum Essential Medium with Earle's Balanced Salts, MEM/EBSS) (Figs. 4a–4c). After the first 100 cycles, the cells remained intact maintaining their original shapes and density on the culture plate (Fig. 4a). However, cell death was observed in the proximity of the device after 500 charge-discharge cycles in Fig. 4b center image and rightmost image where the blue dots (stained with trypan blue) above the white dashed line indicate the dead cells. This result indicates that for the current density of 2 A/g, 100 cycles (762 seconds) has a negligible cytotoxic effect on the cells, but an extended cycling time (3723 seconds for 500 cycles) has toxic effects on the cells in the vicinity of the device. We suspect

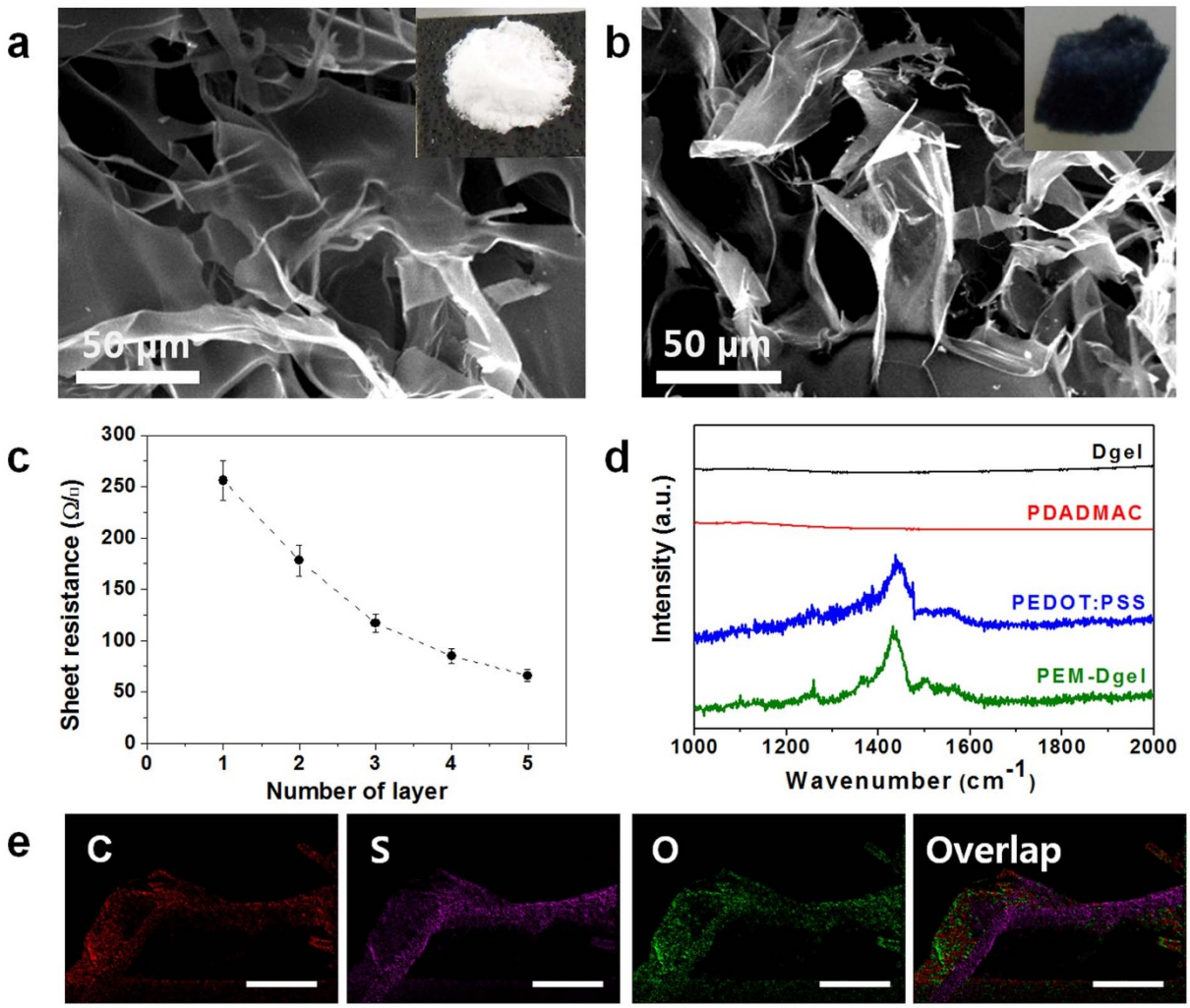

Figure 2 | Morphological, electrical and optical properties. (a), (b), SEM images of Dgel and PEM-Dgel (insets are the digital camera images), (c), Sheet resistance of the PEM_n-Dgel (n = 1.0–5.0); Error bars represent standard deviations from three replicates, (d), Raman spectra of the $PEM_{1.0}$-Dgel and its constituent components (Dgel, PDADMAC, and PEDOT:PSS) for comparison (top), (e), EDS map of $PEM_{1.0}$-Dgel with carbon, oxygen, and sulfur atoms. The scale bar indicates 20 μm. A uniform coating of conductive PEDOT:PSS on the Dgel surface was confirmed by the EDS analysis based on S atoms.

that the osmotic pressure changes induced by the locally elevated concentration of salts diffusing out of both the Dgel and the PEMs cause this damage to the cells. Another reason might be that the PEDOT:PSS leaked out of the PEMs during the cycling, contaminating the environment around the cells. However, as shown in Fig. 4c, the subsequent 500 cycles (for a device that had already been submitted to 500 cycles) had no negative effect on cell viability, indicating the initial 500 cycles acted as a precleaning process for the device by removing the concentrated salt or loosely bound PEDOT:PSS, thus resolving the cytotoxicity problems with our supercapacitor. This non-cytotoxicity of our device is also confirmed with other cell culture media (Dulbecco's Modified Eagle Medium with HDF Human dermal fibroblast cells and Roswell Park Memorial Institute medium with COS7 Monkey kidney fibroblast cells) where precleaning applied devices did not cause the cell death at 1,000 charge-discharge cycles for both case (Fig. S3). In addition to the cytotoxicity, the supercapacitor performance of our device was also studied by cyclic voltammetry in the same cell culture medium. The specific capacitance of PEM-Dgel at 25 mV/s in cell culture medium was measured to be 25.5 ± 2.2 F/g. The dependence of the scan rate on the specific capacitance in the cell medium was also measured. When the scan rate increased from 25 mV/s to 500 mV/s, the specific capacitance was maintained up to 84% in the cell culture medium (Fig. 4e), whereas for PBS and artificial urine, the capacitance decreased to 14% (Fig. 3c). Additionally, the shapes of the CV curves in the cell culture medium were much closer to the ideal rectangle (if we define the fill factor parameter η, where $\eta = \frac{\text{Closed area of CV curve}}{I_{max}V_{max}}$, I_{max} and V_{max} denote the maximum current density measured and the maximum applied voltage, respectively, then $\eta_{cell\ medium} = 0.76$ and $\eta_{PBS} = 0.39$). This result indicates that certain electrolytes present in the cell culture medium readily diffuse into the PEM-Dgel at significantly faster rate than the electrolytes in PBS and artificial urine. The galvanostatic measurements revealed similar behavior: the reduction in the specific capacitance as a function of the current density markedly decreased until 4 A/g. This is remarkably different from the trends observed for PBS and artificial urine (Fig. S4). Although more research is needed to determine the detailed mechanisms, these electrochemical studies demonstrate that our supercapacitor functions well in biological environments.

Discussion

Finally, the electrochemical performance of our PEM-Dgel supercapacitor was evaluated with different number of PEM in a conventional

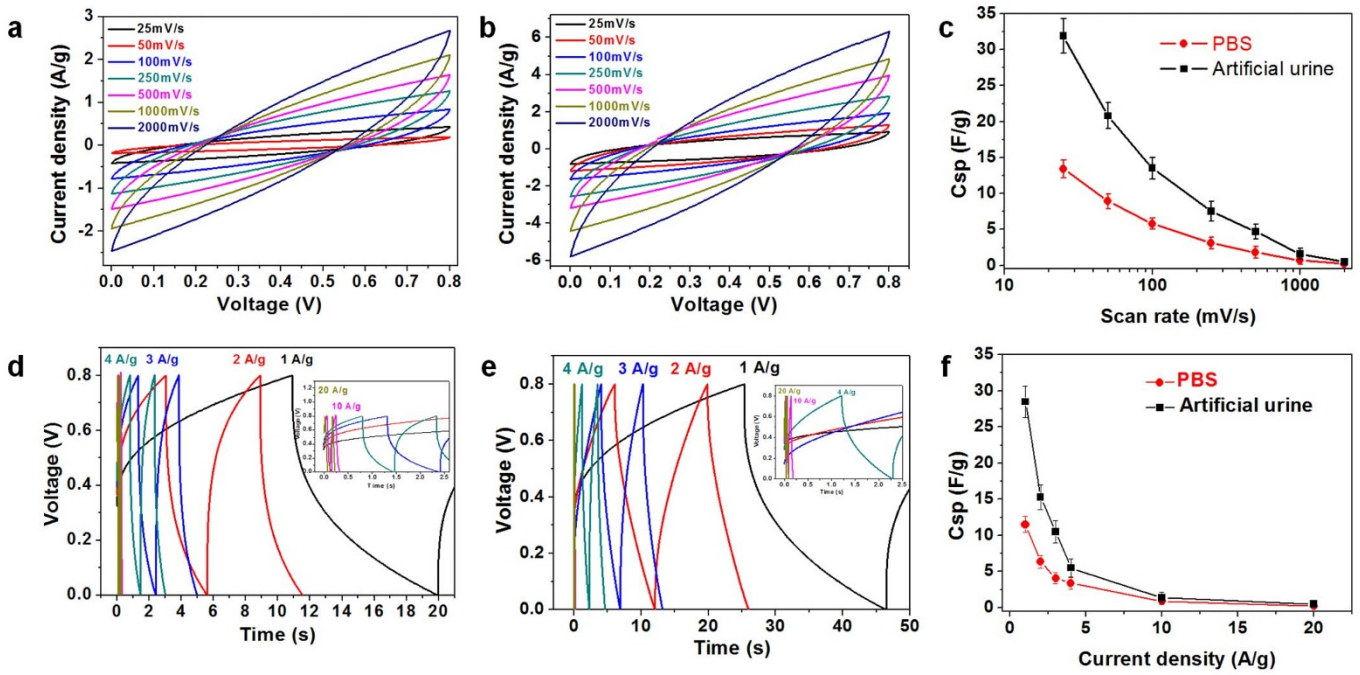

Figure 3 | Electrochemical performance for PEM-Dgel in PBS and artificial urine. (a), (b), Cyclic voltammograms of PEM-Dgel at different voltage scan rates (25 mV/s ~ 2000 mV/s) in PBS and artificial urine, respectively; (d), (e), galvanostatic charge-discharge curves of PEM-Dgel at different current densities (1 A/g ~ 20 A/g) in PBS and artificial urine, respectively; (c), (f), Specific capacitances as a function of the voltage scan rates obtained from the CV data and the current densities obtained from the charge–discharge data, respectively. The insets in d, e present magnified portions of the curves for 10 A/g and 20 A/g in each plot. Error bars represent standard deviations from three replicates.

optimized electrolyte, in this case H_2SO_4, to make a comparison of performances between bioenvironments and fully optimized non-bioenvironments. The specific capacitance of the PEM-Dgel was improved by the formation of multiple polyelectrolyte double layers on the Dgel (PEM_n-Dgel, n = 1.0–5.0) with repeated LBL deposition steps. As shown in Fig. 5a, the specific capacitance increased almost linearly as the number of PEMs increased to three. When five PEMs were deposited onto the Dgel, the specific capacitance of the PEM-Dgel approached the saturated value of approximately 57.4 ± 4.2 F/g at 25 mV/s (Fig. 5b, inset). The increase in the specific capacitance due to the increased number of polyelectrolyte layers was the result of decreased electrochemical resistance (Fig. S5), which may compensate for the mass increase that resulted from the deposition of additional polymer layers. This positive effect was observed for up to three PEMs, but when additional layers were deposited, the capacitance gain was almost equivalent to the mass increase, and the specific capacitance reached a saturated value after the deposition of three layers. We observed similar electrochemical behavior during our galvanostatic charge–discharge experiments, in which the saturation of the discharge time was observed when the number of PEMs was greater than three (Fig. S6). In this case, for reasons similar to those for the changes in the CV data for different numbers of PEMs, the effective contribution of the buildup of conductive material for higher numbers of PEMs was almost negligible. As shown in the Ragone plot for the PEM-Dgel with 1–5 layers (Fig. S7), the power density and the energy density simultaneously and linearly increased as the number of PEMs increased. The electrochemical performance of PEM-Dgel could be further improved by employing a pseudocapacitance material. We coated manganese oxide onto the $PEM_{5.0}$ layer using an electroless plating method in which the $KMnO_4$ precursor was reduced to manganese oxide particles on the outer layer of PEM-Dgel (details of the characterization of manganese oxide are presented in Fig. S8). As a result, the specific capacitance of $PEM_{5.0}/Mn_3O_4$-Dgel was 99.5 ± 7.8 F/g with 2.2 mg/cm^2 of active material, which is 1.7 times higher than that of $PEM_{5.0}$-Dgel at 25 mV/s due to a synergetic charge-transfer redox reaction involving Mn_3O_4. This maximum specific capacitance obtained by full optimization of our device in a harsh environment is only 3.2 fold difference (when compared with specific capacitance in artificial urine at the same operation conditions), which reflects the acceptable performances of our device even in a bioenvironments. The relatively low energy density of supercapacitors is not a critical issue in bioenvironments because the energy demands of devices implanted in the human body are typically low.

The beneficial effect of the higher number of PEMs was also confirmed by the charge-discharge cycling measurements for the $PEM_{1.0}$-, $PEM_{3.0}$-, and $PEM_{5.0}$-Dgels (Fig. 5c). When the number of cycles reached 1000, the capacitance decreased to 70.8, 84.4, and 88.9% of the original capacitance for $PEM_{1.0}$-, $PEM_{3.0}$-, and $PEM_{5.0}$-Dgel, respectively. After 500 cycles, a difference in stability was present between the $PEM_{3.0}$- and $PEM_{5.0}$-Dgel, and this difference increased during further cycling. Because the capacitance difference between the PEM-Dgels with three layers and those with five layers is trivial, the improved mechanical stability of the $PEM_{5.0}$-Dgel, which provides more PEM protection to the Dgel, might be the main factor that contributes to the cycling stability. Fig. 5d compares the cycling stabilities of $PEM_{5.0}$-Dgel in PBS, artificial urine, cell culture medium, and H_2SO_4. In all of the biofluids, the cycling stability of PEM-Dgel device shows the markedly superior behavior to that operated in a non-biofluid. At 1000 cycles, the capacitance retention drops only 5.0, 5.8, and 6.1% for PBS, artificial urine, and cell culture medium, respectively, whereas it increases up to 11.1% for H_2SO_4. These results suggest that our device maintains a great performance level in most biological environments without sacrificing much specific capacitance. Considering the difficulty of multiple implantations in *in vivo* applications, this excellent cycling stability in most biofluids is pivotal advantage of our device as an energy storage device in bioenvironments.

In summary, we developed the supercapacitors which can be directly dipped in physiological fluids in a packageless form and be operated with a great performance. In cell culture medium, PEM-

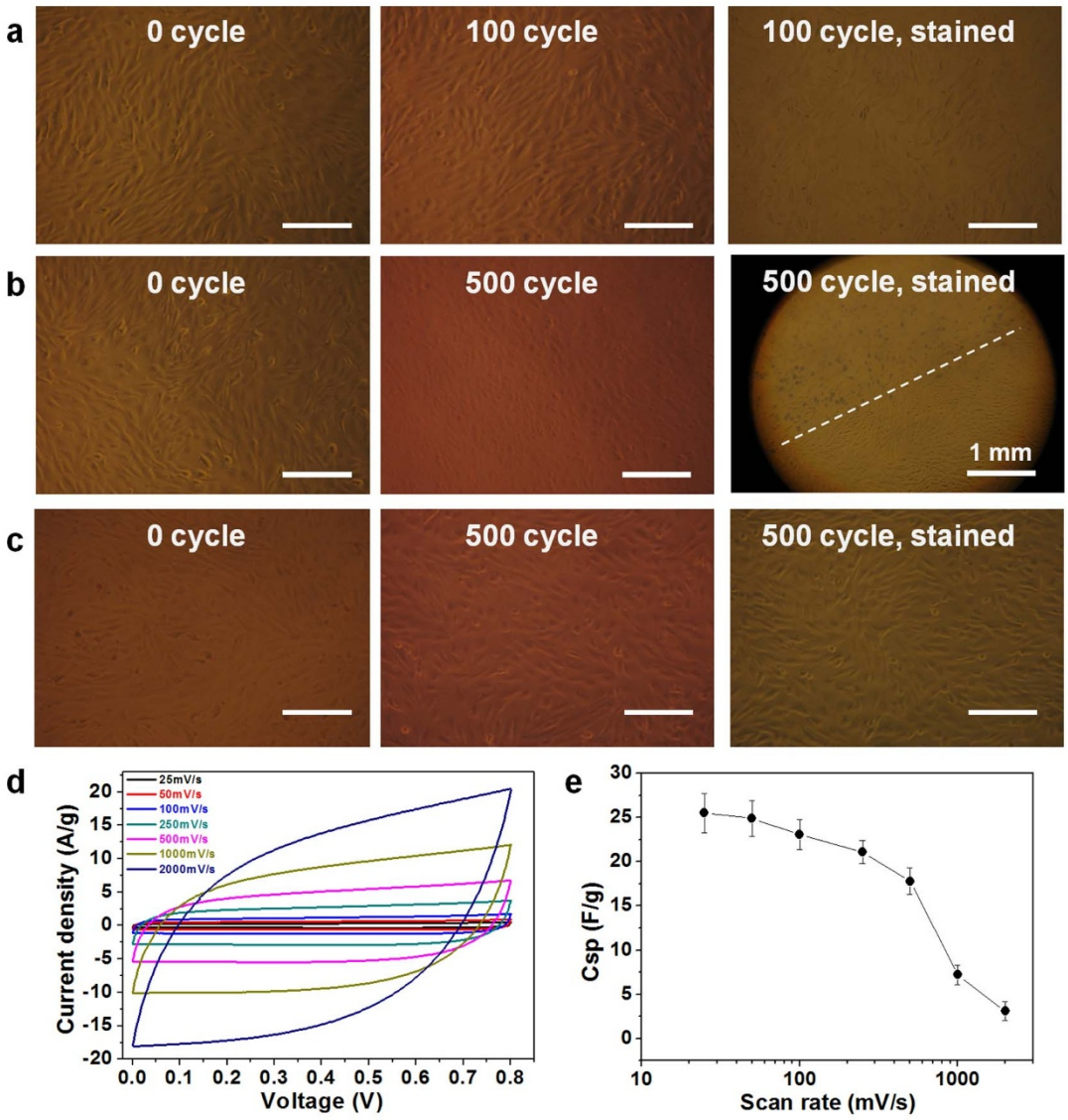

Figure 4 | Cytotoxicity and electrochemical performances of PEM-Dgel in cell culture medium. (a), (b), (c), Optical microscopy images of NIH3T3 cells taken before (1st column) after (2nd column) 100, 500, and 500 cycles with an initial 500 cycles for PEM-Dgel, respectively. The images in the 3rd column are the stained cells with trypan blue for better discrimination of dead cells (above the white dashed line of B). (d), Cyclic voltammograms of PEM-Dgel at different voltage scan rates (25 mV/s ~ 2000 mV/s) in cell culture medium (MEM/EBSS), (e), Specific capacitance variation as a function of the scan rate. Scale bar: 100 μm for all images except that for staining after 500 cycles in panel b. Error bars represent standard deviations from three replicates.

Dgel supercapacitors functioned well without exhibiting any cytotoxic effects after an initial cleaning process was applied. The introduction of nonbiological fluids and Mn_3O_4 does not significantly enhance the performances of our supercapacitors. Rather, the specific capacitance retention is significantly improved when our device is operated in biofluids. Thus, in the near future, we envision that the Dgel-based supercapacitor can be potentially used as a packageless and implantable energy storage device which can be operated in bioenvironments.

Methods

Preparation of the Dgels. The Dgels were synthesized according to previously reported methods[9,15,16]. The X-shaped DNA monomers were fabricated by annealing four single-stranded oligonucleotides that are partially complementary to each other. The Dgel was fabricated by ligating 10 nmol of the X-DNA monomers using 6 units of T4 DNA ligase (Promega) at 16°C for 12 hr.

Polyelectrolyte multilayer deposition. PDADMAC (MW 100,000–200,000 g/mol, Sigma-Aldrich) and PEDOT:PSS (PH 1000, Heraeus) were used as the positive and negative polyelectrolytes, respectively. A 20 mM solution of PDADMAC in deionized sterile water (Bioneer) was used, and PEDOT:PSS was used with the addition of 5 wt% DMSO to achieve a high conductivity[35]. The negatively charged Dgel was immersed in a positively charged PDADMAC solution for 30 min to ensure the complete adsorption of the positive PE. A 200 μL aliquot of water was carefully and repeatedly pipetted into the centrifuge tube (Eppendorf, 1.5 mL) to remove the excess loosely bound PDADMAC. The thoroughly cleaned PDADMAC-coated Dgel was frozen at −20°C for 6 hr and then freeze-dried at −80°C overnight using an ultra-low-temperature freezer (Operon). The completely dried PDADMAC-coated Dgel was immersed in a PEDOT:PSS solution for 30 min. Subsequently, the same sequence of dipping, washing, and freeze-drying of {PDADMAC/PEDOT:PSS} was repeated to deposit the desired number of PEMs.

Fabrication of the electrochemical cell. Without the use of additional binder materials, two PEM-Dgels were cast on gold or copper foil (thickness of 0.127 mm, Alfa Aesar) with an active area of 0.25 cm^2. PEM-Dgel was cast by means of freeze-drying to minimize the morphological change. Whatman filter paper (Advantec 131) was used as a separator between two PEM-Dgels. The device was wrapped in a paraffin film or a 3 M tape to allow good contact. For dipping in PBS (Gibco, pH 7.4) and artificial urine (composed of 1.1 mM lactic acid, 2.0 mM citric acid, 25 mM sodium bicarbonate, 2.5 mM calcium chloride, 90 mM sodium chloride, 2.0 mM magnesium sulfate, 10 mM sodium sulfate, 7.0 mM potassium dihydrogen

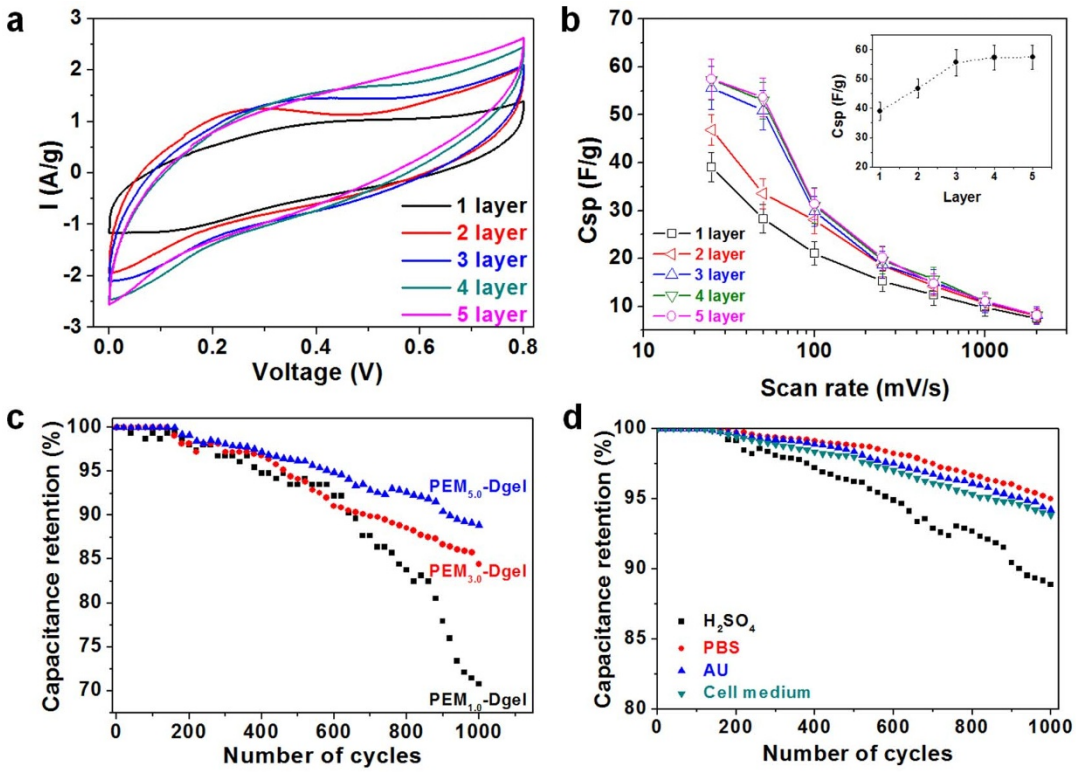

Figure 5 | Optimization of the PEM-Dgel device performance. (a), Cyclic voltammograms of PEM_n-Dgel (n = 1–5) at 25 mV/s, (b), Specific capacitances as a function of the voltage scan rate obtained from the CV data. Loading of active material is 0.4, 0.8, 1.2, 1.6, and 2.0 mg/cm^2 for PEM_n-Dgel (n = 1–5), respectively. Inset indicates the variation in the specific capacitance values with the number of PEMs estimated from each curve, (c), (d), Cyclic stabilities for PEM_n-Dgel (n = 1, 3, and 5) in H_2SO_4 and for $PEM_{5.0}$-Dgel in PBS, artificial urine, cell culture medium, and H_2SO_4, respectively. Error bars represent standard deviations from three replicates.

phosphate, 7.0 mM dipotassium hydrogen phosphate, 25 mM ammonium chloride, and 170 mM urea), the devices were sealed in a poly bag (Sigma-Aldrich). For dipping in cell culture medium (MEM/EBSS, 10% fetal bovine serum + 1% penicillin), the device was directly immersed in the cell culture medium without sealing. The device was carefully placed on mouse embryonic fibroblast cells (NIH3T3 cells) to avoid causing mechanical damage to the cells.

Electrochemical performance measurements. Cyclic voltammograms (CVs) and galvanostatic charge–discharge curves were measured using a BioLogic HCP803 potentiostat/galvanostat. During the CV measurements, a potential range of 0.0 to 0.8 V was applied under a voltage sweep rate of 25–2000 mV/s. The specific capacitance was calculated from both the CV curve and the discharge curve of the galvanostatic charge–discharge data using the following equation:

$$C_{sp} = \int_{V_1}^{V_2} \frac{I(V)}{2(V_2 - V_1)\nu M} dV \quad (1)$$

where V_1, V_2, ν, and M are the starting voltage, the ending voltage, the voltage scan rate, and the total mass of the active materials, respectively, and

$$C_{sp} = -\frac{I}{(\Delta V/\Delta t)M} \quad (2)$$

where I, ΔV, Δt, and M are the applied current, the voltage, the time, and the total mass of the active electrode materials (PEM-Dgel), respectively.

The internal resistance was calculated from the initial voltage drop in the discharge curve using the equation

$$R = \frac{\Delta V_{IR}}{2I} \quad (3)$$

where ΔV_{IR} is the IR drop and I is the applied current.

The power and energy densities were determined using the following equations:

$$P = \frac{V^2}{4RM} \quad (4)$$

$$E = \frac{1}{2M} CV^2 \quad (5)$$

where V, R, M, and C are the applied potential, the internal resistance, the total mass of the active electrode materials, and the measured capacitance of the cell, respectively. The cycling test was performed at 2 A/g with a cutoff potential of 0.8 V.

Electroless deposition of Mn_3O_4. PEM-Dgel was immersed in a 6 mM aqueous $KMnO_4$ solution for 30 min to allow the thorough infiltration of the Mn_3O_4 precursor ions. The reducing agent, 12 mM $NH_2OH{\cdot}HCl$ solution, was added for 30 min to produce Mn_3O_4 particles. The initially purple solution became brown as the reduction reaction proceeded. The Mn_3O_4 particles deposited within the PEM-Dgel were gently washed with DI water to remove Mn_3O_4 aggregates from the bulk solution. The PEM/Mn_3O_4-Dgel was then freeze-dried as described in the PEM deposition procedure.

Characterization of the sample morphologies by SEM. The Dgel, PEM-Dgel, and PEM/Mn_3O_4-Dgel were analyzed using a field-emission scanning electron microscope (SEM, Hitachi S-4700, operation voltage of 15 keV). Platinum was sputtered onto the Dgel as a conductive coating for imaging purposes, and the PEM-Dgel and PEM/Mn_3O_4-Dgel samples were imaged without a conductive coating. Elemental maps using EDS were obtained based on C, O, and S atoms to identify the PEDOT:PSS distribution on the Dgel.

Cytotoxicity of the PEM-Dgel supercapacitor. NIH3T3 mouse embryonic fibroblast cells, HDF Human dermal fibroblast cells and COS7 Monkey kidney fibroblast cells were purchased from the Korean Cell Line Bank. NIH3T3 cells were maintained in Minimum Essential Medium with Earle's Balanced Salts (Hyclone), HDF cells were maintained in Dulbecco's Modified Eagle Medium (Hyclone), and COS7 cells were maintained in Roswell Park Memorial Institute medium (Hyclone), all supplemented with 10% fetal bovine serum (Hyclone) and 1% penicillin streptomycyin (Hyclone). Cells were grown in a 6-well plate at a density of 1×10^5 cells/well at 37°C under 5% CO_2. After 2 days, cells were exposed to a number of charging-discharging cycles via direct contact with the electrode. Then they were stained with 0.4% trypan blue (GIBCO) for 5 min to reveal the cell mortality with blue staining. Cellular images were taken before and after trypan blue treatments using Zeiss Axiovert 40 CFL with 10× objective lens.

Raman spectroscopy and X-ray diffraction. Raman scattering spectra with a resolution of approximately 1 cm^{-1} were collected in a backscattering configuration at room temperature using a Renishaw inVia Raman microscope. The samples were illuminated with a 514 nm He–Ne laser (power: 4 mW) on a Leica microscope with a 20× objective. Powder X-ray diffraction (XRD) patterns were collected to analyze the

phases of the samples using an X-ray diffractometer (Philips) equipped with a Cu Kα radiation source (λo = 1.5418 Å).

Measurement of the sheet resistance. The sheet resistances of the PEM-Dgel and the PEM/Mn_3O_4-Dgel were measured using the four-point probe method (Hall Measurement System, Nanometrics) with an HL5500WIN Hall System, ver 2.23.

1. Zhang, Y. & Seeman, N. C. Construction of a DNA-Truncated Octahedron. *J. Am. Chem. Soc.* **116**, 1661–1669 (1994).
2. He, Y. *et al.* Hierarchical self-assembly of DNA into symmetric supramolecular polyhedra. *Nature* **452**, 198–202 (2008).
3. Li, Y. *et al.* Controlled assembly of dendrimer-like DNA. *Nature Mater.* **3**, 38–42 (2004).
4. Goodman, R. P. *et al.* Reconfigurable, braced, threedimensional DNA nanostructures. *Nature Mater.* **3**, 93–96 (2008).
5. Gu, H., Chao, J., Xiao, S. & Seeman, N. C. Dynamic patterning programmed by DNA tiles captured on a DNA origami substrate. *Nature Nanotech.* **4**, 245–248 (2009).
6. Aldaye, F. A. *et al.* Modular construction of DNA nanotubes of tunable geometry and single- or doublestranded character. *Nature Nanotech.* **4**, 349–352 (2009).
7. Han, D., Pal, S., Liu, Y. & Yan, H. Folding and cutting DNA into reconfigurable topological nanostructures. *Nature Nanotech.* **5**, 712–717 (2010).
8. Aldaye, F. A., Palmer, A. L. & Sleiman, H. F. Assembling Materials with DNA as the Guide. *Science* **321**, 1795–1799 (2008).
9. Um, S. *et al.* Enzyme-catalysed assembly of DNA hydrogel. *Nature. Mater.* **5**, 797–801 (2006).
10. Peppas, N. A., Hilt, J. Z., Khademhosseini, A. & Langer, R. Hydrogels in Biology and Medicine: From Molecular Principles to Bionanotechnology. *Adv. Mater.* **18**, 1345–1360 (2006).
11. Elisseeff, J. Hydrogels: Structure starts to gel. *Nature Mater.* **7**, 271–273 (2008).
12. Lutolf, M. Biomaterials: Spotlight on hydrogels. *Nature Mater.* **8**, 451–453 (2009).
13. Zhang, S. Hydrogels: Wet or let die. *Nature Mater.* **3**, 7–8 (2004).
14. Kloxin, A. M., Kasko, A. M., Salinas, C. N. & Anseth, K. Photodegradable hydrogels for dynamic tuning of physical and chemical properties. *Science* **324**, 59–63 (2009).
15. Park, N., Um, S., Funabashi, H., Xu, J. & Luo, D. A cell-free protein producing gel. *Nature. Mater.* **8**, 432–437 (2009).
16. Park, N. *et al.* High-yield cell-free protein production from P-gel. *Nature Protocol* **4**, 1759–1770 (2009).
17. Koschwanez, H. E. & Reichert, W. M. In vitro, in vivo and post explanation testing of glucose-detecting biosensors: current methods and recommendations. *Biomaterials* **28**, 3687–3703 (2007).
18. Frazier, O. H. & Jacob, L. P. Small pumps for ventricular assistance: progress in mechanical circulatory support. *Cardiol. Clin.* **25**,553–564 (2007).
19. Kim, D. *et al.* Blossey, Materials for multifunctional balloon catheters with capabilities in cardiac electrophysiological mapping and ablation therapy. *Nature. Mater.* **10**, 316–323 (2011).
20. Bettinger, C. J. & Bao, Z. Organic thin-film transistors fabricated on resorbable biomaterial substrates. *Adv. Mater.* **22**, 651–655 (2010).
21. Prokop, A. Bioartificial organs in the twenty-first century: nanobiological devices. *Ann. N. Y. Acad. Sci.* **944**, 472–490 (2001).
22. Burgess, D. J. *et al.* A Review of the Biocompatibility of Implantable Devices: Current Challenges to Overcome Foreign Body Response. *J. Diabetes Sci. Technol.* **2**, 1003–1015 (2008).
23. Simon, P. & Gogotsi, Y. Materials for electrochemical capacitors. *Nature. Mater.* **7**, 845–854 (2008).
24. Maier, J. Nanoionics: ion transport and electrochemical storage in confi ned systems. *Nature Mater.* **4**, 805–815 (2005).
25. Arico, A. S. *et al.* Nanostructured materials for advanced energy conversion and storage devices. *Nature Mater.* **4**, 366–377 (2005).
26. Pan, L. *et al.* Hierarchical nanostructured conducting polymer hydrogel with high electrochemical activity. *Proc. Natl. Acad. Sci.* **109**, 9287–9292 (2012).
27. Jeong, H. M. *et al.* Nitrogen-doped graphene for high performance ultracapacitors and the importance of nitrogen-doped sites at basal-planes. *Nano Lett.* **11**, 2472–2477 (2011).
28. Choi, B. G. *et al.* 3D Macroporous Graphene Frameworks for Supercapacitors with High Energy and Power Densities. *ACS Nano.* **6**, 4020–4028 (2012).
29. Rolison, D. R. *et al.* Multifunctional 3D nanoarchitectures for energy storage and conversion. *Chem. Soc. Rev.* **38**, 226–252 (2009).
30. Lang, X., Hirata, A., Fujita, T. & Chen, M. Nanoporous metal/oxide hybrid electrodes for electrochemical supercapacitors. *Nature Nanotech.* **6**, 232–236 (2011).
31. Pushparaj, V. L. *et al.* Flexible energy storage devices based on nanocomposite paper. *Proc. Natl. Acad. Sci.* **104**, 13574–13577 (2007).
32. Hillberg, A. L. & Tabrizian, M. Biorecognition through layer-by-layer polyelectrolyte assembly: In-situ hybridization on living cells. *Biomacromolecules* **7**, 2742–2750 (2006).
33. Sukhorukov, G. B., Mijhwald, H., Decher, G. & Lvov, Y. M. Assembly of polyelectrolyte multilayer films by consecutively alternating adsorption of polynucleotides and polycations. *Thin Solid Films* **284–285**, 220–223 (1996).
34. Stavytska-Barba, M. & Kelley, A. M. Surface-enhanced raman study of the interaction of PEDOT:PSS with plasmonically active nanoparticles. *J. Phys. Chem. C.* **114**, 6822–6830 (2010).
35. Colesmann, A. *et al.* Inverted semi-transparent organic solar cells with spray coated, surfactant free polymer top-electrodes. *Sol. Energ. Mat. Sol. C.* **98**, 118–123 (2012).

Acknowledgments

The authors thank W. Paek and D. Yu for their assistance with the SEM imaging, EDS mapping and XRD experiments.

Author contributions

J.H. and N.P. designed the experiments. J.H., K.I., S.H., S.K. and N.P. performed the experiments and analyzed the data. J.H., K.I., S.H. and N.P. wrote the manuscript. B.C., S.H. and K.K. provided advice on the project.

Additional information

Supplementary information accompanies this paper at http://www.nature.com/scientificreports

Competing financial interests: The authors declare no competing financial interests.

How to cite this article: Hur, J. *et al.* DNA hydrogel-based supercapacitors operating in physiological fluids. *Sci. Rep.* **3**, 1282; DOI:10.1038/srep01282 (2013).